# Can substitutions affect the oxidative stability of lithium argyrodite solid electrolytes?

Ananya Banik,<sup>a</sup> Yunsheng Liu,<sup>b</sup> Saneyuki Ohno,<sup>c</sup> Yannik Rudel,<sup>a</sup> Alberto Jiménez-Solano,<sup>d</sup> Andrei Gloskovskii,<sup>e</sup> Nella M. Vargas-Barbosa,<sup>f</sup> Yifei Mo,<sup>b</sup>\* and Wolfgang G. Zeier<sup>a,f</sup>\*

<sup>a</sup>Institute of Inorganic and Analytical Chemistry, University of Münster, Corrensstrasse 30, 48149 Münster, Germany.

<sup>b</sup>Department of Materials Science and Engineering, University of Maryland, College Park, Maryland 20742, United States.

<sup>c</sup>Department of Applied Chemistry, Graduate School of Engineering, Kyushu University, 744 Motooka, Nishi-ku, 819-0395 Fukuoka, Japan.

<sup>d</sup>Max Planck Institute for Solid State Research, Heisenbergstraße 1, 70569 Stuttgart, Germany.

<sup>e</sup>Deutsches Elektronen-Synchrotron DESY 22607, Hamburg, Germany.

<sup>f</sup>Institut für Energie- und Klimaforschung (IEK), IEK-12: Helmholtz-Institut Münster,

Forschungszentrum Jülich, Corrensstrasse 46, 48149 Münster, Germany.

Corresponding authors\*: yfmo@umd.edu, wzeier@uni-muenster.de

**Abstract:** Lithium ion conducting argyrodites are among the most studied solid electrolytes due to their high ionic conductivities. A major concern in a solid-state battery is the solid electrolyte stability. Here we present a systematic study on the influence of cationic and anionic substitution on the electrochemical stability of  $\text{Li}_6\text{PS}_5X$ , using step-wise cyclic voltammetry, optical band gap measurements, hard X-ray photoelectron spectroscopy along with first-principles calculations. We observe that going from  $\text{Li}_6\text{PS}_5\text{Cl}$  to  $\text{Li}_{6+x}\text{P}_{1-x}M_x\text{S}_5\text{I}$  ( $M=\text{Si}^{4+}$ ,  $\text{Ge}^{4+}$ ), the oxidative degradation does not change. Considering the chemical bonding shows that the valence band edges are mostly populated by non-bonding orbitals of the  $\text{PS}_4^{3-}$  units or unbound sulfide anions and that simple substitutions in these sulfide-based solid electrolytes cannot improve oxidative stabilities. This work provides insights on the role of chemical bonding on the stability of superionic conductors and shows that alternative strategies are needed for long-term stable solid-state batteries.

Keywords: Solid electrolyte, electrochemical stability, solid-state battery, lithium ion conducting argyrodite, photoemission spectroscopy

#### 1. Introduction

The all-solid-state battery has garnered interest as a viable alternative to conventional Li-ion batteries. 1,2 Successful production of a solid-state battery requires a solid electrolyte (SE) with high Li-ion conductivity and wide (electro)chemical stability window.<sup>3-5</sup> The lithium-ion conducting thiophosphates are currently used for solid electrolytes due to their high ionic conductivity and mechanical softness.<sup>6–9</sup> Recent efforts have led to the discovery of various thiophosphate electrolytes such as  $\text{Li}_6\text{PS}_5X$  (X = Cl, Br, I),  $^{6,10-13}$   $\text{Li}_{10}M\text{P}_2\text{S}_{12}$  (M = Ge, Sn),  $^{9,14,15}$ and Li<sub>2</sub>S-P<sub>2</sub>S<sub>5</sub> glass-ceramic phases<sup>16</sup>. Nevertheless, the main concern related to the use of these solid electrolytes is a limited understanding of the solid electrolyte - electrode interfacial (in)stability. 17-19 In most cases, the solid electrolyte reacts with electrode materials leading to the formation of passivating interphase layers, similar to what is observed with liquid electrolytes in Li-ion batteries. 19-22 Even though an interphase layer may potentially stop further solid electrolyte degradation and thus enable long-term cycling, solid-state battery performance would be poorer due to the increased cell resistance. Therefore, two routes have emerged to promote long-term cycling that focus either on incorporating protective coatings in active materials 19,23 or utilizing compositional changes in known solid electrolyte phases to achieve higher stabilities<sup>24–26</sup>. While the former option has shown to be very effective, it is unclear if substitution in sulfide solid electrolytes can enhance their stability towards the electrode materials for operation. Further, recent reports have explored the role of electronically insulating additives to improve electrochemical stability of thiophosphates;<sup>27</sup> however the reason behind enhanced stability is not clear yet.

In principle, there are multiple approaches to determine the electrochemical stability window of a solid electrolyte. The stability window is defined as the voltage range in which the electrolyte does not participate in charge-transfer reactions with the electrode materials. In other words, the electrolyte is neither reduced nor oxidized at the electrolyte-electrode interface. The three possible approaches to determine the electrochemical stability windows are (1) the "band edge approach", (2) the "stoichiometry stability approach" and (3) the "phase stability approach". All of these are in-depth described and compared to each other by Binninger et al.<sup>28</sup> The band edge approach (or sometimes called HOMO-LUMO) suggests that to prevent the reduction of a solid electrolyte at the anode, the Fermi level of the anode ( $\varepsilon_{F,anode}$ ) should be at lower energies than the conduction band minimum of the solid electrolyte. Similarly, to prevent oxidative decomposition, the electrochemical potential of the cathode (also its Fermi level,  $\varepsilon_{F,cathode}$ ) should be at a higher energy than the valence band maximum

shown schematically in Figure 1a.29 The energy difference between the conduction band minimum and the valence band maximum is the band gap. This is the reason for the more often used terminology of "band gap approach". Whereas the "stoichiometry stability approach" is mostly used for insertion/extraction reactions, the "phase stability approach" is used to calculate intrinsic thermodynamic stability windows of solid electrolytes. <sup>20,21,28,30</sup> The "phase stability approach" considers the electrolyte as a reactant that can be fully oxidized or reduced to produce specific products at specific (redox) potentials. These decomposition reactions are directly related to the Gibbs free energies of the redox reactions(s). <sup>28,31</sup> In short, the "band edge" approach" is expected to determine which element drives the decomposition and provide an upper limit to the stability window, while the thermodynamic electrochemical stability approach defines the decomposition potential(s) of a solid electrolyte (see Figure 1b). However, it is often observed that the stability windows theoretically predicted tend to be much narrower than those observed experimentally (Figure 1c). 17,18,32,33 The mismatch between theory and experiment is due to the fact that interfacial reaction kinetics and intermediate metastable phases are not fully accounted for in the calculations. 17,34,35 Additionally, different measurement approaches for the stability window can limit comparability. Recent attempts to better determine the experimental electrochemical stability window have used carbon – solid electrolyte composites and then either stepwise cyclic voltammetry<sup>17,18,36</sup> or linear sweep voltammetry<sup>37</sup> to measure these electrochemical stabilities.

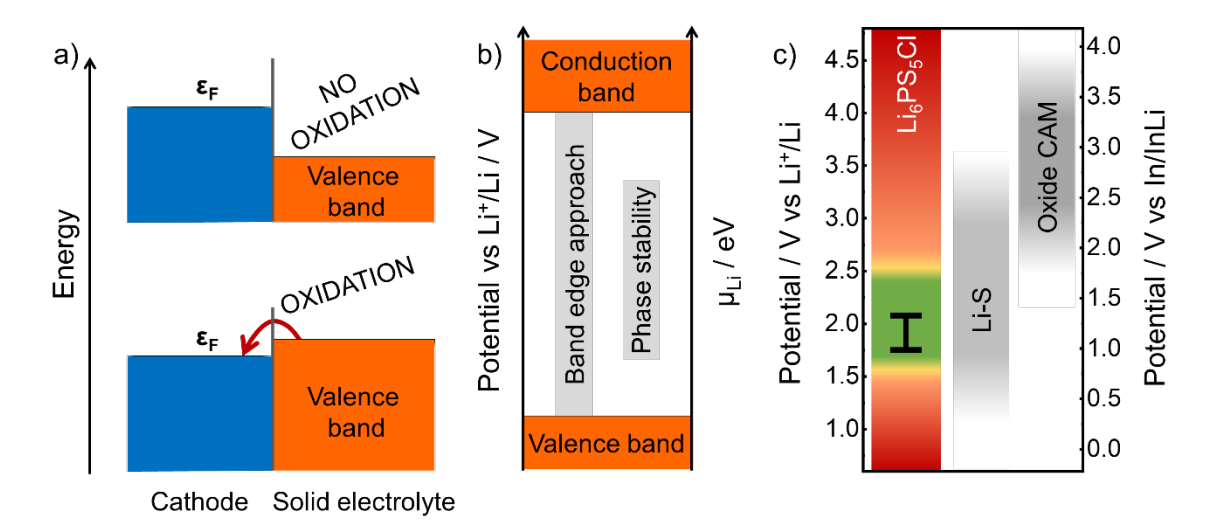


Figure 1. a) Schematic of oxidative degradation mechanism of a solid electrolyte in contact with a cathode active material based on band theory of solids. Oxidative degradation of the solid electrolyte involves electron transfer from the valence band edge to the cathode. Thus, for a stable electrolyte, the valence band minimum needs to be at energies below the Fermi

level  $\varepsilon_F$  of cathode. The atoms that contribute to the band edges participate in the electron transfer process with cathode during decomposition. b) Comparison of typical electrochemical stability window obtained from band gap approach and phase stability method. c) Comparison of practical stability window of Li<sub>6</sub>PS<sub>5</sub>Cl (green colored region) with thermodynamic phase stability (marked by double-headed arrow). Oxidative and reductive decomposition of Li<sub>6</sub>PS<sub>5</sub>Cl is closely related to the sulfur and phosphorous redox potentials. Oxidative decomposition starts at 2.5 V vs In/InLi, whereas reductive decomposition occurs below 0.6 V vs In/InLi.<sup>17</sup> The calculated thermodynamic phase stability window<sup>21</sup> is narrower than the measured one. Typical cycling windows of Li–S and oxide cathode active materials (CAM) are also shown for comparison.

Clearly, solid electrolytes must have an upper bound to their oxidative stability. For instance, in the case of Li<sub>6</sub>PS<sub>5</sub>Cl, its oxidative stability is within the operating voltage range of sulfur as a cathode material, but outside of the typical range of oxide-based insertion cathode active materials (Figure 1c).<sup>17,18</sup> It is therefore critical to elucidate if these argyrodites can be improved to achieve a higher oxidative stability. This question is especially important since tailoring the composition is a typical approach to improve ionic conductivities,<sup>5</sup> yet it is unclear if the stability is also affected.

In order to answer the question if altering the composition affects the oxidative electrochemical degradation, in this work we compare the electrochemical stability of sulfide based argyrodites  $Li_{6+x}MS_5X$  by changing the composition ( $M = P^{5+}$ ,  $Si^{4+}$ ,  $Ge^{4+}$ ;  $X = Cl^-$ ,  $I^-$ ). Using a combination of hard X-ray photoemission spectroscopy to unravel the band edges together with optical band gap measurements, we compare these experimental data to theoretical calculations of the band structure and the phase stability. Additionally, step-wise cyclic voltammetry is used to measure the changes in the practical oxidative stability. Here, we show that changing the composition in these argyrodite-based ionic conductors barely affect the thermodynamic and electrochemical stability. By understanding the chemical nature of the band edges, we show that as long as sulfur is part of the solid electrolyte, the oxidative stability will always be limited, irrespective of the full chemical composition.

# 2. Experimental section

*Synthesis of solid electrolytes*. Li<sub>6</sub>PS<sub>5</sub>Cl, Li<sub>6.6</sub>P<sub>0.4</sub>Si<sub>0.6</sub>S<sub>5</sub>I and Li<sub>6.6</sub>P<sub>0.4</sub>Ge<sub>0.6</sub>S<sub>5</sub>I were synthesized via a classic solid-state reaction as reported before and the diffraction patterns are displayed in Figure S1.<sup>6,8</sup> For the Li<sub>6.6</sub>P<sub>0.4</sub>Ge<sub>0.6</sub>S<sub>5</sub>I synthesis, an additional 3.5 wt% of Li<sub>2</sub>S was used unlike previous report.

*Potentiostatic impedance spectroscopy (PEIS):* Room temperature ionic conductivities were measured by AC impedance spectroscopy on the pellets with vapor-deposited gold layers, using a VMP300 impedance analyzer (Bio-Logic Science Instruments) at frequencies from 7 MHz to 100 mHz with an amplitude of 10 mV. The resulting geometrical densities of the pellets were around 80 % (Table S1). Conductivity values are 1.8, 1.7 and 2.9 mS·cm<sup>-1</sup> for Li<sub>6</sub>PS<sub>5</sub>Cl, Li<sub>6.6</sub>P<sub>0.4</sub>Si<sub>0.6</sub>S<sub>5</sub>I, (denoted as Si-Li<sub>6</sub>PS<sub>5</sub>I) and Li<sub>6.6</sub>P<sub>0.4</sub>Ge<sub>0.6</sub>S<sub>5</sub>I (denoted as Ge-Li<sub>6</sub>PS<sub>5</sub>I), respectively, similar to previous reports (Figure S2).<sup>6–8</sup>

*Optical absorption spectra:* Diffuse reflectance spectra of solid samples were obtained with the aid of an airtight cuvette (Hellma) and an integrated sphere attached to a double monochromator spectrofluorometer (FLS980, Edinburgh Instruments) operating in synchronous mode. The double monochromator setting, both in the excitation and in the collection, discard any photoluminescent signal belongs to the sample. Subsequently, diffuse reflectance spectra were converted using the Kubelka-Munk-function:  $F(R) = \frac{(1-R)^2}{2R}$ . Taucplots were used to determine the band gap taking into account that the argyrodites have a direct band gap.

Hard X-ray photoemission spectra (HAXPES): Room temperature hard X-ray photoelectron spectroscopy measurements were performed at the P22 beamline at PETRA III, Deutsches Elektronen-Synchrotron, Hamburg using 6 keV X-rays to measure bulk electronic structure of Li<sub>6</sub>PS<sub>5</sub>X.<sup>38</sup> A Si (333) post-monochromator was used, the overall energy resolution was set to 150 meV. The spectra were recorded with a Phoibos 225 HV electron energy analyzer from SPECS Surface Nano Analysis GmbH. To avoid air exposure, the pelletized samples were transferred from a glovebox to the analysis chamber using a transfer vessel filled with argon gas. The X-rays were incident at almost grazing angle (85°) and the data were acquired in nearly normal emission geometry. All spectra were calibrated with respect to the binding energy of Au 4f<sub>7/2</sub> at 84.0 eV. Charge corrections were done using C1s binding energy line (binding energy: 284.6 eV) corresponding to aliphatic carbon.

*Preparation of SE-carbon composite cathode:* Commercial carbon black with a BET-determined surface area of 1300 m<sup>2</sup>·g<sup>-1</sup> (ECP600JD, LION, Ltd.) was used as electronically conducting component of the working electrode composite. ECP600JD was dried in a Büchi oven at 300 °C for 24 h under dynamic vacuum before composite cathode preparation. To prepare SE-C electrode composite, SE and carbon were mixed in a weight ratio of 9:1 and ball-milled for 24 cycles in 80 mL vessel with ZrO<sub>2</sub> milling media (diameter of 5 mm) under Aratmosphere. Each cycle consists of 10 min running at a rotation speed of 600 rpm and 10 min rest. The ball-milled composite was extracted from the vessel and used as cathode for electrochemical stability testing.

Cyclic voltammetry (CV): Step-wise cyclic voltammetry was used to measure the oxidative stability window using the press cell set up.18 First, 80 mg of SE was filled into the PEEK housing and handpressed with stainless steel stamps. 12 mg of SE-C composite was put onto the SE pellet followed by uniaxial pressing for 3 min at 35 kN using an electronic press to prepare the working electrode. Next, a 100 µm thick indium (In) foil (chemPUR, 99.995%) of 9 mm diameter was placed on the opposite side of the SE separator layer as counter electrode. Finally, the cell was fixed in an aluminum frame with a torque of 10 Nm, resulting in a pressure of approximately 60 MPa. Here, In metal was used as the reference electrode instead of lithium to ensure no reductive degradation of SE due to presence of additional lithium source during the electrochemical study. Indium metal establishes an equilibrium potential of 0.62 V vs. Li<sup>+</sup>/Li due to lithiation with SE, thus lithiated In was the reference electrode here as shown previously. 18,39 The stepwise CV experiments were performed using a VMP-300 potentiostat (Biologic) with steps of 0.1 V where the upper reversal potential was varied from 1.6 to 3.0 V vs. In/InLi with scan rate of 0.1 mV/s. For Si-Li<sub>6</sub>PS<sub>5</sub>I and Ge-Li<sub>6</sub>PS<sub>5</sub>I, we have additionally measured CV with 0.05 V step in 1.7-1.9 V to understand the change in decomposition voltage due to substitution. All steps were started as anodic sweeps from the open-circuit potential (OCV) and carried out twice consecutively (Figure S3).

Computational methods: All density functional theory (DFT) calculations were performed using the Vienna ab initio simulation package<sup>40</sup> (VASP) with the projector augmented-wave<sup>41</sup> (PAW) approach. Generalized-gradient approximation (GGA) and Perdew-Burke-Ernzerhof<sup>42</sup> (PBE) functionals were adopted to calculate the total energy, the energy above the hull  $E_{\text{hull}}$ , and the electrochemical windows. The Heyd-Scuseria-Ernzerhof<sup>43</sup> (HSE) functionals were used to calculate the density of states (DOS) and corresponding band gaps of materials. All static DFT calculations were spin-polarized and used convergence parameters consistent with

the *Materials Project* (MP),<sup>44,45</sup> except that the energy convergence (EDIFF) and the force convergence (EDIFFG) parameters were set to 10<sup>-7</sup> eV and 0.01 eV/Å respectively when calculating DOS and band gaps, to get highly accurate electronic structures. All DFT calculations were generated and analyzed using the Python Materials Genomics (pymatgen) library.<sup>46</sup>

Representative ordered structures of each composition with site partial occupancy were generated as follows. 10,000 ordered structures were constructed, where all disordered sites were randomly occupied using partial occupancies as the probabilities of being occupied. 20 symmetrically distinct structures among the 10,000 ordered structures were selected with minimal electrostatic energies for further calculations. The final structure with the lowest DFT energy among the 20 selected structures were used as the representative ordered structure of the compound.

The calculations of electrochemical stability and windows were performed using grand potential phase diagrams following the schemes established in previous studies. All compounds and their corresponding energies in grand potential phase diagrams were obtained from the MP database and the grand potential phase diagram was constructed by pymatgen. All entries in the grand potential phase diagram were selected with the 'theoretical' label in MP database set to false. The grand potential phase diagram identified the phases with the lowest energy at given composition with an open reservoir of Li with chemical potential  $\mu_{\text{Li}}$ , which was a function of applied potential  $\varphi$  referenced to Li metal, with the relation  $\mu_{\text{Li}}(\varphi) = \mu_{\text{Li}}^0 - e\varphi$ , following the established scheme in previous studies. The range of  $\varphi$ , where the corresponding compounds of interest were neither oxidized nor reduced, were the calculated electrochemical windows. For those compounds with the positive energies above the convex hull,  $E_{\text{hull}}$ , the convex hull energies of the compounds were used to evaluate phase stability and their electrochemical stability in the grand potential phase diagrams.

All analysis on crystal orbital Hamilton population (COHP) were performed using software Local-Orbital Basis Suite Towards Electronic-structure Reconstruction<sup>50</sup> (LOBSTER), and the corresponding input files with calculation parameters were generated by pymatgen, following similar process in previous studies.<sup>51</sup> The static DFT calculations of structure relaxation for COHP analysis were implemented using energy convergence set to  $10^{-7}$  eV and force convergence set to 0.01 eV/Å.

#### 3. Results and discussion

Lithium-ion conducting halide argyrodites, Li<sub>6</sub>PS<sub>5</sub>X have been of particular interest because of their high ionic conductivity, their negligible grain boundary resistance, and the possibility to change the ionic conductivity via substitutions. The oxidative decomposition pathway of Li<sub>6</sub>PS<sub>5</sub>Cl has been explored in depth, <sup>17,18</sup> and the underlying chemical reactions occur due to the sulfur being readily oxidized. Li<sub>6</sub>PS<sub>5</sub>Cl consists of PS<sub>4</sub><sup>3-</sup> *ortho*-thiophosphate species, together with S<sup>2-</sup> and Cl<sup>-</sup> anions. At the stability limit, the oxidative degradation involves the oxidation of PS<sub>4</sub><sup>3-</sup> and S<sup>2-</sup> anions, forming polysulfides, sulfur and additional (P-S)<sub>x</sub> units. <sup>18,19</sup> After decomposition, these units themselves become redox active. <sup>18</sup>

In order to understand how compositional substitutions change the oxidative stability of these argyrodites, we employ Li<sub>6</sub>PS<sub>5</sub>Cl as the baseline material and use substituted-Li<sub>6</sub>PS<sub>5</sub>I, Li<sub>6.6</sub>P<sub>0.4</sub>Si<sub>0.6</sub>S<sub>5</sub>I and Li<sub>6.6</sub>P<sub>0.4</sub>Ge<sub>0.6</sub>S<sub>5</sub>I as additional model systems. We aim to elucidate how the oxidative stability is affected in argyrodites by employing cationic substitution, replacing P with Si or Ge, and anionic substitution, exchanging Cl with I. The Ge and Si substituted model systems have been chosen due to their similar ionic conductivities,<sup>6,8,39</sup> which allow for the experimental measurement of the electrochemical stability and excludes mass-transport effects as an influencing factor. Unfortunately, the low ionic conductivity of unsubstituted Li<sub>6</sub>PS<sub>5</sub>I excludes it from electrochemical measurements,<sup>52</sup> nevertheless for the theoretical work it was used as an additional benchmark to compare the direct change from Li<sub>6</sub>PS<sub>5</sub>Cl to Li<sub>6</sub>PS<sub>5</sub>I.

Practical electrochemical stability. To understand the influence of the composition on the electrochemical stability, we determine the stability limit using a step-wise cyclic voltammogram approach, that has recently been shown to be effective for elucidating the stability of sulfide solid electrolytes. <sup>17,18</sup> Since the oxidative stability of Li<sub>6</sub>PS<sub>5</sub>X is the major concern for its usage in a solid-state battery, here we focus on the oxidative degradation only. Carbon – solid electrolyte composites are used to enhance the interfacial areas. The voltammogram is recorded twice up to this reversal potential followed by a stepwise increase of the potential range by 0.1 V up to 3 V vs. In/InLi (Figure 2 and Figure S3). As seen in Figure 2a-c, below a certain voltage (1.8 V vs In/InLi), only a capacitive current can be observed. After that, with increasing voltage, a significant increase in current was observed. The peak current of each scan rises drastically when increasing the reversal voltage above 1.8 V vs In/InLi. Additionally, after the decomposition, anodic and cathodic features start to evolve indicating the known redox-activity of the decomposition products. <sup>18</sup> Typically, for Li<sub>6</sub>PS<sub>5</sub>Cl,

oxidative decomposition occurs near 2.5 V vs Li<sup>+</sup>/Li.<sup>18</sup> When the measured current increases as a function of the potential (Figure 2d), all systems show similar onsets of decomposition by increasing currents. In other words, the oxidative stability window does not change abruptly from Li<sub>6</sub>PS<sub>5</sub>Cl to substituted Li<sub>6</sub>PS<sub>5</sub>I indicating that neither the anion nor the cation substitutions affect the practical oxidative electrochemical stability.

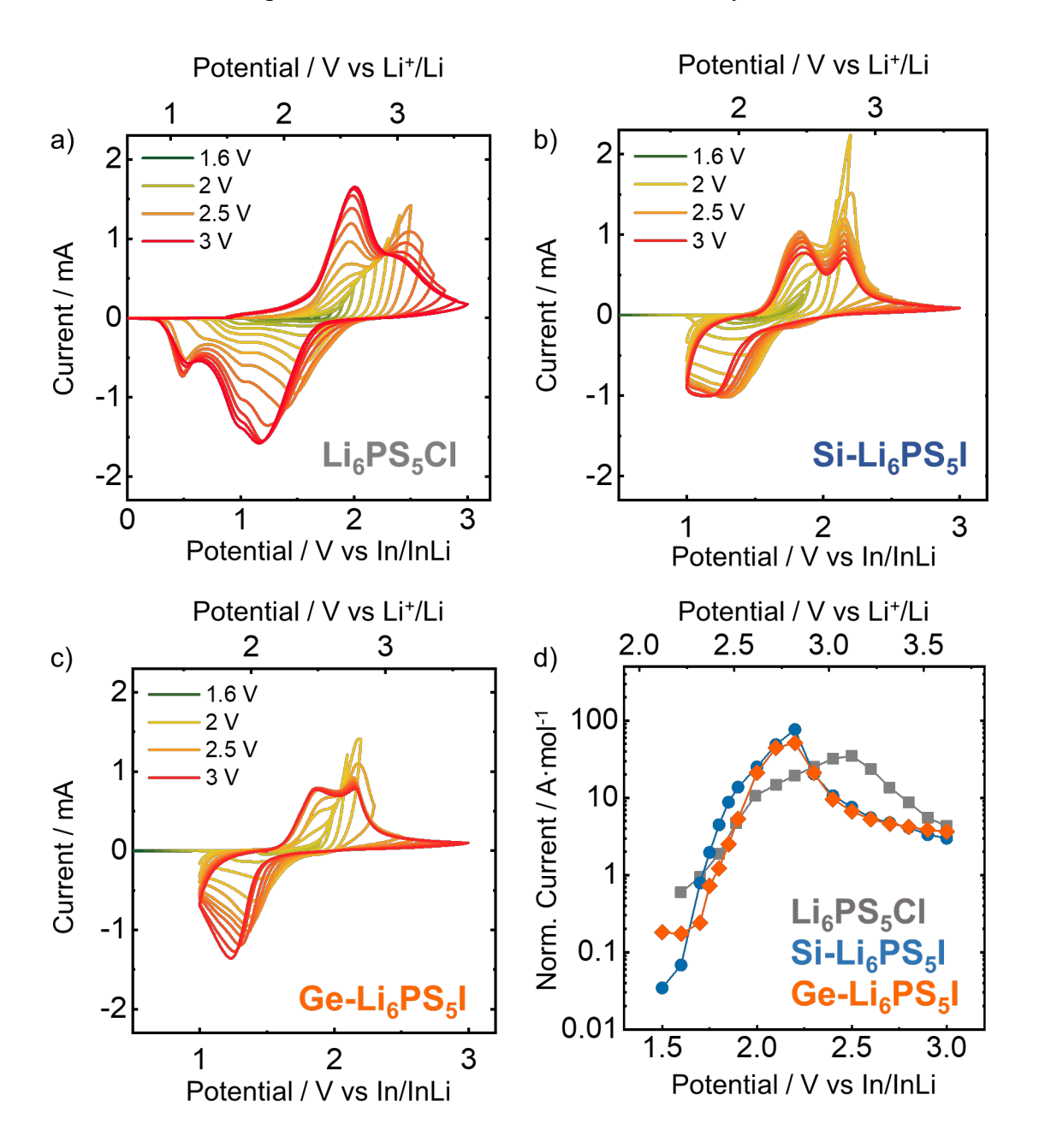


Figure 2. Stepwise cyclic voltammogram for  $Li_6PS_5Cl$ ,  $Si-Li_6PS_5I$  and  $Ge-Li_6PS_5I$  (a, b and c). Oxidative decomposition at high potentials leads to evolving peaks with varying peak area at potentials at which the electrolyte was apparently stable when lower reversal potentials were applied. Open-circuit voltage was 0.5 V vs. In/InLi. The change in the upper reversal potential

is represented by a color gradient. For better visualization several potential steps (potential vs In/InLi) are marked. d) Comparison of oxidative currents at reversal potentials of CV scans normalized by moles of material to decouple from potential compositional differences.

Measuring band edges and calculating stability windows. Although there are a few reports on the understanding of electronic structure and how it influences the (electro)chemical stability, there are no experimental studies focusing on the chemical nature of the band edges and their relation to the electrochemical decomposition of solid electrolytes. We have measured the optical band gap and valence band spectra to shed light on the electronic structure of these materials (Figure 3a and b). All the materials exhibit direct band gap values with above 3 eV, similar to the ones observed theoretically (Figure 3a and Table S2). The large band gap values are also in line with poor electronic conductivity ( $\sim 10^{-8} \text{ S} \cdot \text{cm}^{-1}$ ) of these materials. <sup>53–55</sup> Hard Xray photoemission spectroscopy (HAXPES) is a common tool to visualize the valence band edge of bulk material.<sup>56</sup> While it is primarily used in semiconductors with high electronic conductivities, its usage is rare in studies of ionic conductors. To avoid the surface contribution, we have used X-ray with high energy (6 keV) which is a typical energy source used to probe bulk materials.<sup>38</sup> Unfortunately, no HAXPES data collection was possible for Li<sub>6</sub>PS<sub>5</sub>I, due to strong sample changing. Figure 3b shows the valence band photoelectron spectra for Li<sub>6+x</sub>P<sub>1-</sub>  $_{x}M_{x}S_{5}X$ . The HAXPES features correspond to electronic density of occupied states near Fermi level. According to Figure 3b, for all the materials, the first peak appears at a similar energy, suggesting similar valence band edge energies of these electronic insulators. To understand the electronic structure and its impact on redox activity, we have calculated the electronic structure using density functional theory. We have chosen the compositions of Li<sub>6.25</sub>P<sub>0.75</sub>Si<sub>0.25</sub>S<sub>5</sub>I and Li<sub>6.75</sub>P<sub>0.25</sub>Ge<sub>0.75</sub>S<sub>5</sub>I as Si- and Ge- substituted Li<sub>6</sub>PS<sub>5</sub>I for theoretical calculation since these are the nearest to the actual composition of experimentally prepared compounds.<sup>6,8</sup> Both valence band maxima and conduction band minima occur at the  $\Gamma$ -point, confirming direct band gap, as seen in Figure S4. From the electronic structure calculations, diffuse reflectance spectra and HAXPES measurements it is clear that the valence band maxima do not change significantly upon substitution. Slight shifts in the band gap are observed which can hence be associated with the change in the conduction band position upon cationic substitution.

To understand the thermodynamics of the electrochemical degradation pathway, we have calculated the lithium evolution number as a function of potential (Figure S5). From these calculations we obtain the thermodynamic stability window shown in Figure 3c, with the thermodynamic decomposition products listed in Table S3. In direct comparison, the here

determined practical electrochemical stability windows (Figure 3d) closely resemble the calculated stability window, albeit a slightly larger stability. Unlike previous reports, <sup>18</sup> the reaction kinetics were enhanced with the use of a highly conducting higher surface area carbon, leading to a better comparison to experiment. Interestingly, Li<sub>6</sub>PS<sub>5</sub>I seems to exhibit a slightly higher thermodynamic stability than the substituted ones, making Li<sub>6</sub>PS<sub>5</sub>I an intermediate degradation product for the decomposition of Ge-Li<sub>6</sub>PS<sub>5</sub>I. From the thermodynamic decomposition products it is clear that decomposition of these sulfide solid electrolyte leads to formation of electrochemically active compounds such as sulfur, leading to the observed redox behavior as shown in Figure 2. <sup>18</sup> Besides, LiX is found as one of the decomposition products, which has been recently proved to enhance the oxidative stability of thiophosphate, Li<sub>3</sub>PS<sub>4</sub>. <sup>27</sup>

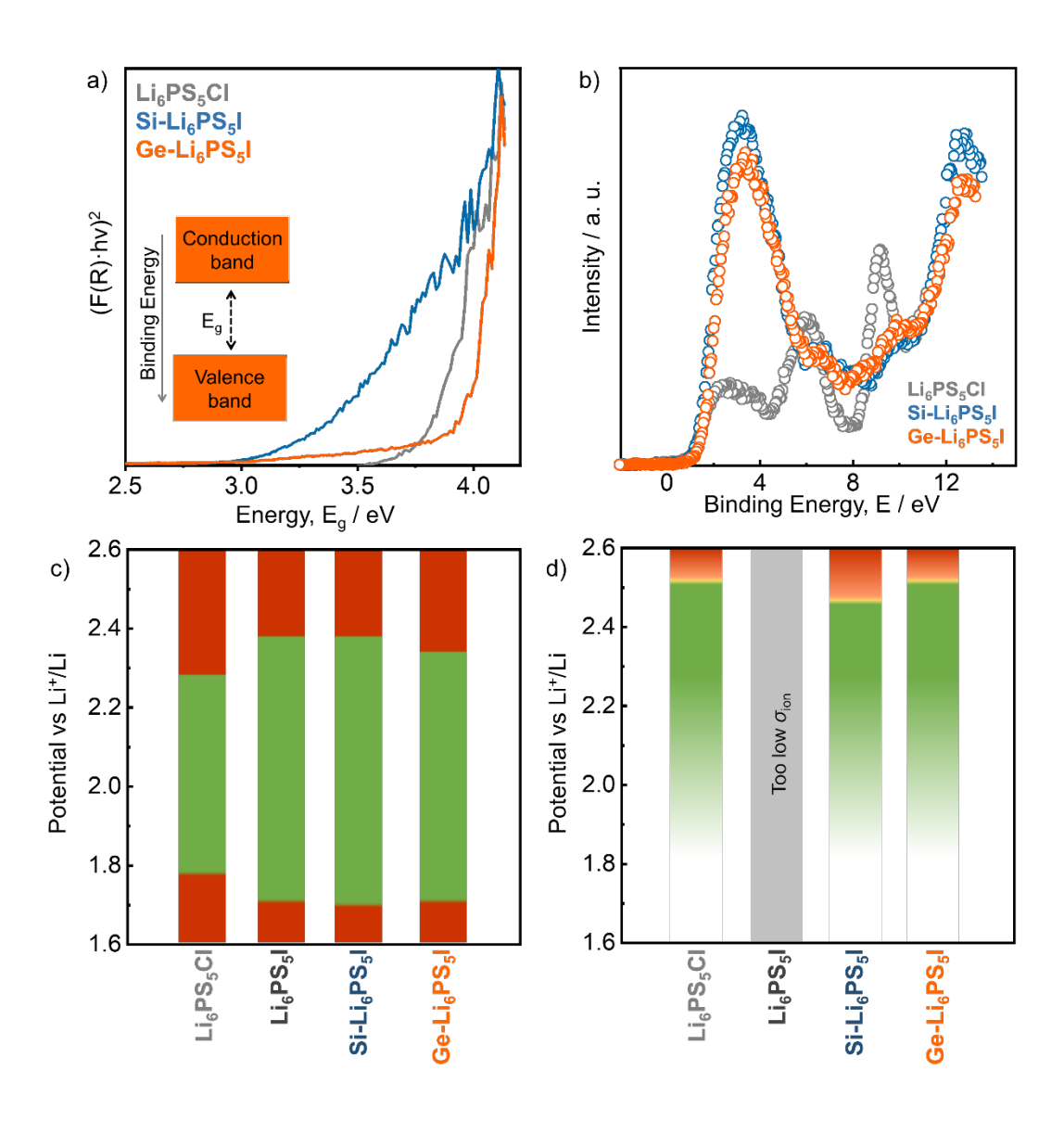


Figure 3. a) Optical absorption spectra and b) hard X-ray photoemission spectra showing band gap,  $E_g$  and valence band edges, respectively. c) Calculated thermodynamic electrochemical

stability windows and d) experimental oxidative stability limits. The stable region for each electrolyte is shown in green and the onset of oxidative decomposition is shown in orange followed by red to show the unstable potential region. Because of a too low ionic conductivity  $(\sigma_{ion})$   $Li_6PS_5I$  cannot be studied via the CV measurements.

Clearly the substitutions via the halide anion or substitution of the cation in PS43- units do not significantly affect the stability of these sulfide argyrodites solid ionic conductors. To shed light on the relation between electronic structure and electrochemical stability, we take a closer look at the contributions of all atoms to the band edges. Partial density of states (pDOS) as well as crystal orbital Hamilton populations (COHP) were calculated for all the compounds (Figure 4 and Figure S6). These contributions can be qualitatively understood considering a simplified schematic of pDOS (Figure 4a) considering the valence state energy states based the electronegativity of the atoms and with it their atomic orbital energies. Whereas the pDOS give an idea of the atomic contributions to the different bands and electronic states, the COHP provide information about which states exhibit bonding or anti-bonding chemical interactions. Considering the pDOS, in all the investigated lithium argyrodites the valence bands are mostly composed of anion states, of which sulfur seems to dominate the valence band edge. In the case of Li<sub>6</sub>PS<sub>5</sub>Cl the Cl-states are located deeper in the valence band, whereas for the I-based materials the halide states can also be found at the valence band edge (Figure S6). It is noteworthy that this stronger influence of the halide at the band edge seems to be reflected in the HAXPES data in which the I-based materials exhibit a stronger intensity at the band edge (see Figure 3b and Figure S6). Nevertheless, the sulfur states contribute the most states to the valence band edge, irrespective of the halide composition. In line with the thermodynamic phase equilibria calculation, I<sup>-</sup>/I<sub>2</sub> redox does not influence the electrochemical stability window of argyrodite solid electrolytes (Table S4) and can be neglected. In the conduction band, the cationic contributions, especially those from P, are stronger leading to nearly equal contributions of S, suggesting an even stronger influence of PS<sub>4</sub><sup>3-</sup> on the conduction band edge. This is corroborated by the COHP which highlights the contributions of PS<sub>4</sub><sup>3-</sup> units on the electronic structure. The conduction band edge is populated mainly with P-S antibonding states while the P-S bonding states lie far below the valence band edge. Since the P-S bonding states of the PS<sub>4</sub><sup>3-</sup> units are so low in energy, this means that the filled non-bonding sulfur orbitals express as heavy states in the electronic structure and form the valence band edge for these materials. In Li<sub>6</sub>PS<sub>5</sub>Cl, the higher electronegativity of chlorine shifts the 3p states below the valence band edge. For the iodide materials, even though both the free sulfur and iodine contributes to the valence band edge, the major contribution comes from non-bonding *p*-states of the sulfur atoms of PS<sub>4</sub><sup>3-</sup> unit and the S<sup>2-</sup> anion in the structure. These bonding considerations show that even if substitutions are performed on the MS<sub>4</sub> units or the halide composition, the energy state of the valence band maximum is mostly determined by the sulfur states. Upon substitution of P with more electropositive Ge/Si, an additional M-S bonding state forms just above the P-S state, as seen in Figure S6 (d and f). Therefore, substitutions can only affect the magnitude of the band gaps as stronger bonding interactions in the MS<sub>4</sub> units would then shift the conduction band minimum to higher energies, as reflected in the measured optical band gaps.

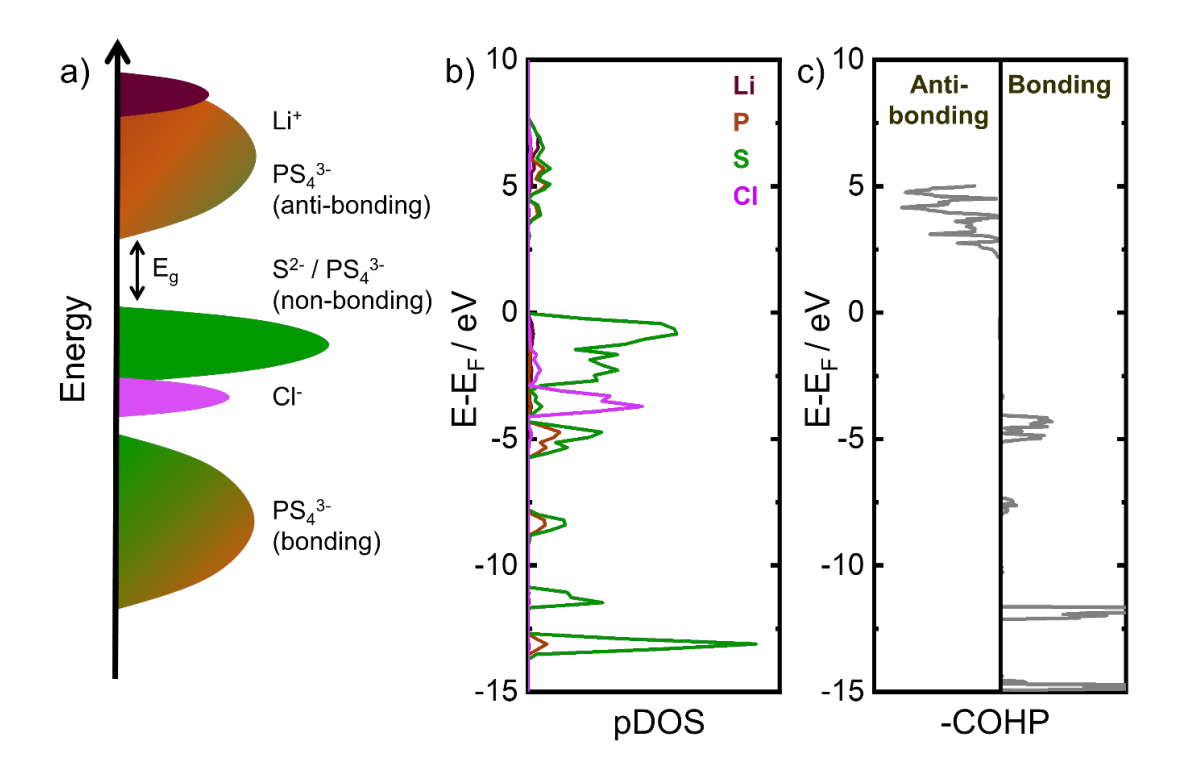


Figure 4. Electronic structure of  $Li_6PS_5Cl$ . a) Schematic of pDOS showing major contribution of free  $S^{2-}$  and non-bonding sulfur states from the  $PS_4^{3-}$  unit in the valence band edge, whereas the conduction band is dominated by antibonding states of  $PS_4^{3-}$ . Because of a larger electronegativity, the  $Cl^-$  states reside deeper in the valence and do not participate in bonding with phosphorous. The  $PS_4^{3-}$  bonding states are far below the valence band maximum. b) Partial, atom-projected DOS shows the  $PS_4^{3-}$  unit along with free  $S^{2-}$  and  $Cl^-$  make up the valence band. c) Crystal Orbital Hamilton populations (COHP) shows the bonding – antibonding contributions of  $PS_4^{3-}$  in the electronic structure.

These electronic structure considerations of the argyrodites show why substitutions in argyrodite-based materials are hardly affecting the oxidative stability of the materials. Sulfur states dominate the band edge, effectively pinning the oxidative stability window. Thus, one can expect a similar oxidative stability for all sulfide solid electrolytes, regardless of the full composition. As the exact thermodynamic stability is linked to the decomposition pathways, minor changes in oxidative stability are expected, however, the driving force for the decomposition remains at the sulfur band edges.

#### Conclusion

In summary, we use a combination of electronic structure calculations, thermodynamic phase stability calculations along with experimental determination of band edges and effective oxidative stability windows in the argyrodite family of superionic conductors. By elucidating the chemical nature of the band edges and developing an in-depth understanding of the bonding interactions, we demonstrate sulfur to be the Achilles' heel of the oxidative stability of sulfide solid electrolytes. Our results show that simple substitutions in sulfide solid electrolytes can barely change their intrinsic oxidative electrochemical stability, and with it the decomposition pathways, if sulfur remains part of the chemical composition. Therefore, for long-term stable operation of solid-state batteries, cathode active material coatings or different materials classes are needed altogether.

#### **Additional Information**

#### **Notes**

The authors declare no conflict of interest.

## **ACKNOWLEDGMENTS**

The research was supported by the Federal Ministry of Education and Research (BMBF) within project FESTBATT under grant number 03XP0430F. This research used resources at the P22 beamline at the light source PETRA III of DESY, a member of the Helmholtz Association (HGF). A. B. and S. O. gratefully acknowledge the Alexander von Humboldt Foundation for financial support through a Postdoctoral Fellowship. Y.L and Y.M acknowledge the funding support from National Science Foundation HDR Program under award number 1940166, and the computational facilities from the University of Maryland supercomputing resources and the Maryland Advanced Research Computing Center (MARCC).

### SUPPORTING INFORMATION

Laboratory X-ray diffraction data along with Pawley fit; room temperature impedance spectra; comparison of maximum currents at reversal potential during CV; electronic structures; Lithium-evolution number vs voltage plot; pDOS and COHP; band gap; phase equilibria at the reduction and oxidation potentials of the solid electrolyte; phase equilibria at different applied potentials

#### References

- (1) Janek, J.; Zeier, W. G. A Solid Future for Battery Development. *Nat. Energy* **2016**, *1* (9), 16141.
- (2) Randau, S.; Weber, D. A.; Kötz, O.; Koerver, R.; Braun, P.; Weber, A.; Ivers-Tiffée, E.; Adermann, T.; Kulisch, J.; Zeier, W. G.; Richter, F. H.; Janek, J. Benchmarking the Performance of All-Solid-State Lithium Batteries. *Nat. Energy* **2020**, *5* (3), 259–270.
- (3) Wang, Y.; Richards, W. D.; Ong, S. P.; Miara, L. J.; Kim, J. C.; Mo, Y.; Ceder, G. Design Principles for Solid-State Lithium Superionic Conductors. *Nat. Mater.* 2015, 14 (10), 1026–1031.
- (4) Culver, S. P.; Koerver, R.; Krauskopf, T.; Zeier, W. G. Designing Ionic Conductors: The Interplay between Structural Phenomena and Interfaces in Thiophosphate-Based Solid-State Batteries. *Chem. Mater.* **2018**, *30* (13), 4179–4192.
- (5) Ohno, S.; Banik, A.; Dewald, G. F.; Kraft, M. A.; Krauskopf, T.; Minafra, N.; Till, P.; Weiss, M.; Zeier, W. G. Materials Design of Ionic Conductors for Solid State Batteries. *Prog. Energy* **2020**, *2* (2), 022001.
- (6) Kraft, M. A.; Ohno, S.; Zinkevich, T.; Koerver, R.; Culver, S. P.; Fuchs, T.; Senyshyn, A.; Indris, S.; Morgan, B. J.; Zeier, W. G. Inducing High Ionic Conductivity in the Lithium Superionic Argyrodites Li<sub>6+x</sub>P<sub>1-x</sub>Ge<sub>x</sub>S<sub>5</sub>I for All-Solid-State Batteries. *J. Am. Chem. Soc.* **2018**, *140* (47), 16330–16339.
- (7) Kraft, M. A.; Culver, S. P.; Calderon, M.; Böcher, F.; Krauskopf, T.; Senyshyn, A.; Dietrich, C.; Zevalkink, A.; Janek, J.; Zeier, W. G. Influence of Lattice Polarizability on the Ionic Conductivity in the Lithium Superionic Argyrodites Li<sub>6</sub>PS<sub>5</sub>X (X = Cl, Br, I). *J. Am. Chem. Soc.* **2017**, *139* (31), 10909–10918.

- (8) Ohno, S.; Helm, B.; Fuchs, T.; Dewald, G.; Kraft, M. A.; Culver, S. P.; Senyshyn, A.; Zeier, W. G. Further Evidence for Energy Landscape Flattening in the Superionic Argyrodites Li<sub>6+x</sub>P<sub>1-x</sub>M<sub>x</sub>S<sub>5</sub>I (M = Si, Ge, Sn). *Chem. Mater.* **2019**, *31* (13), 4936–4944.
- (9) Kamaya, N.; Homma, K.; Yamakawa, Y.; Hirayama, M.; Kanno, R.; Yonemura, M.; Kamiyama, T.; Kato, Y.; Hama, S.; Kawamoto, K.; Mitsui, A. A Lithium Superionic Conductor. *Nat. Mater.* **2011**, *10* (9), 682–686.
- (10) Adeli, P.; Bazak, J. D.; Park, K. H.; Kochetkov, I.; Huq, A.; Goward, G. R.; Nazar, L. F. Boosting Solid-State Diffusivity and Conductivity in Lithium Superionic Argyrodites by Halide Substitution. *Angew. Chemie Int. Ed.* 2019, 58 (26), 8681–8686.
- (11) Gautam, A.; Sadowski, M.; Prinz, N.; Eickhoff, H.; Minafra, N.; Ghidiu, M.; Culver, S. P.; Albe, K.; Fässler, T. F.; Zobel, M.; Zeier, W. G. Rapid Crystallization and Kinetic Freezing of Site-Disorder in the Lithium Superionic Argyrodite Li<sub>6</sub>PS<sub>5</sub>Br. *Chem. Mater.* **2019**, *31* (24), 10178–10185.
- (12) Zhou, L.; Minafra, N.; Zeier, W. G.; Nazar, L. F. Innovative Approaches to Li-Argyrodite Solid Electrolytes for All-Solid-State Lithium Batteries. *Acc. Chem. Res.* **2021**, *54* (12), 2717–2728.
- (13) Zhou, L.; Assoud, A.; Zhang, Q.; Wu, X.; Nazar, L. F. New Family of Argyrodite Thioantimonate Lithium Superionic Conductors. *J. Am. Chem. Soc.* **2019**, *141* (48), 19002–19013.
- (14) Krauskopf, T.; Culver, S. P.; Zeier, W. G. Bottleneck of Diffusion and Inductive Effects in Li<sub>10</sub>Ge<sub>1-x</sub>Sn<sub>x</sub>P<sub>2</sub>S<sub>12</sub>. *Chem. Mater.* **2018**, *30* (5), 1791–1798.
- (15) Culver, S. P.; Squires, A. G.; Minafra, N.; Armstrong, C. W. F.; Krauskopf, T.; Böcher, F.; Li, C.; Morgan, B. J.; Zeier, W. G. Evidence for a Solid-Electrolyte Inductive Effect in the Superionic Conductor Li<sub>10</sub>Ge<sub>1-x</sub>Sn<sub>x</sub>P<sub>2</sub>S<sub>12</sub>. J. Am. Chem. Soc. 2020, 142 (50), 21210–21219.
- (16) Dietrich, C.; Weber, D. A.; Sedlmaier, S. J.; Indris, S.; Culver, S. P.; Walter, D.; Janek, J.; Zeier, W. G. Lithium Ion Conductivity in Li<sub>2</sub>S-P<sub>2</sub>S<sub>5</sub> Glasses-Building Units and Local Structure Evolution during the Crystallization of Superionic Conductors Li<sub>3</sub>PS<sub>4</sub>, Li<sub>7</sub>P<sub>3</sub>S<sub>11</sub> and Li<sub>4</sub>P<sub>2</sub>S<sub>7</sub>. *J. Mater. Chem. A* **2017**, *5* (34), 18111–18119.

- (17) Ohno, S.; Rosenbach, C.; Dewald, G. F.; Janek, J.; Zeier, W. G. Linking Solid Electrolyte Degradation to Charge Carrier Transport in the Thiophosphate-Based Composite Cathode toward Solid-State Lithium-Sulfur Batteries. *Adv. Funct. Mater.* 2021, 2010620.
- (18) Dewald, G. F.; Ohno, S.; Kraft, M. A.; Koerver, R.; Till, P.; Vargas-Barbosa, N. M.; Janek, J.; Zeier, W. G. Experimental Assessment of the Practical Oxidative Stability of Lithium Thiophosphate Solid Electrolytes. *Chem. Mater.* **2019**, *31* (20), 8328–8337.
- (19) Walther, F.; Koerver, R.; Fuchs, T.; Ohno, S.; Sann, J.; Rohnke, M.; Zeier, W. G.; Janek, J. Visualization of the Interfacial Decomposition of Composite Cathodes in Argyrodite-Based All-Solid-State Batteries Using Time-of-Flight Secondary-Ion Mass Spectrometry. *Chem. Mater.* 2019, 31 (10), 3745–3755.
- (20) Richards, W. D.; Miara, L. J.; Wang, Y.; Kim, J. C.; Ceder, G. Interface Stability in Solid-State Batteries. *Chem. Mater.* **2016**, *28* (1), 266–273.
- (21) Zhu, Y.; He, X.; Mo, Y. Origin of Outstanding Stability in the Lithium Solid Electrolyte Materials: Insights from Thermodynamic Analyses Based on First-Principles Calculations. *ACS Appl. Mater. Interfaces* **2015**, 7 (42), 23685–23693.
- (22) Xiao, Y.; Wang, Y.; Bo, S. H.; Kim, J. C.; Miara, L. J.; Ceder, G. Understanding Interface Stability in Solid-State Batteries. *Nat. Rev. Mater.* **2020**, *5* (2), 105–126.
- (23) Culver, S. P.; Koerver, R.; Zeier, W. G.; Janek, J. On the Functionality of Coatings for Cathode Active Materials in Thiophosphate-Based All-Solid-State Batteries. *Adv. Energy Mater.* **2019**, *9* (24), 1900626.
- (24) Asano, T.; Sakai, A.; Ouchi, S.; Sakaida, M.; Miyazaki, A.; Hasegawa, S. Solid Halide Electrolytes with High Lithium-Ion Conductivity for Application in 4 V Class Bulk-Type All-Solid-State Batteries. *Adv. Mater.* **2018**, *30* (44), 1803075.
- (25) Schlem, R.; Muy, S.; Prinz, N.; Banik, A.; Shao-Horn, Y.; Zobel, M.; Zeier, W. G. Mechanochemical Synthesis: A Tool to Tune Cation Site Disorder and Ionic Transport Properties of Li<sub>3</sub>MCl<sub>6</sub> (M = Y, Er) Superionic Conductors. *Adv. Energy Mater.* 2020, 10, 1903719.
- (26) Li, X.; Liang, J.; Yang, X.; Adair, K. R.; Wang, C.; Zhao, F.; Sun, X. Progress and Perspectives on Halide Lithium Conductors for All-Solid-State Lithium Batteries.

- Energy Environ. Sci. 2020, 13, 1429-1461.
- (27) Hakari, T.; Fujita, Y.; Deguchi, M.; Kawasaki, Y.; Otoyama, M.; Yoneda, Y.; Sakuda, A.; Tatsumisago, M.; Hayashi, A. Solid Electrolyte with Oxidation Tolerance Provides a High- Capacity Li<sub>2</sub>S-Based Positive Electrode for All-Solid-State Li / S Batteries. *Adv. Funct. Mater.* **2021**, 2106174.
- (28) Binninger, T.; Marcolongo, A.; Mottet, M.; Weber, V.; Laino, T. Comparison of Computational Methods for the Electrochemical Stability Window of Solid-State Electrolyte Materials. *J. Mater. Chem. A* **2020**, *8* (3), 1347–1359.
- (29) Goodenough, J. B.; Park, K. S. The Li-Ion Rechargeable Battery: A Perspective. *J. Am. Chem. Soc.* **2013**, *135* (4), 1167–1176.
- (30) Zhu, Y.; He, X.; Mo, Y. First Principles Study on Electrochemical and Chemical Stability of Solid Electrolyte–electrode Interfaces in All-Solid-State Li-Ion Batteries. *J. Mater. Chem. A* **2016**, *4* (9), 3253–3266.
- (31) Peljo, P.; Girault, H. H. Electrochemical Potential Window of Battery Electrolytes: The HOMO-LUMO Misconception. *Energy Environ. Sci.* **2018**, *11* (9), 2306–2309.
- (32) Tan, D. H. S.; Wu, E. A.; Nguyen, H.; Chen, Z.; Marple, M. A. T.; Doux, J. M.; Wang, X.; Yang, H.; Banerjee, A.; Meng, Y. S. Elucidating Reversible Electrochemical Redox of Li<sub>6</sub>PS<sub>5</sub>Cl Solid Electrolyte. *ACS Energy Lett.* **2019**, *4*, 2418–2427.
- (33) Schwietert, T. K.; Arszelewska, V. A.; Wang, C.; Yu, C.; Vasileiadis, A.; de Klerk, N. J. J.; Hageman, J.; Hupfer, T.; Kerkamm, I.; Xu, Y.; van der Maas, E.; Kelder, E. M.; Ganapathy, S.; Wagemaker, M. Clarifying the Relationship between Redox Activity and Electrochemical Stability in Solid Electrolytes. *Nat. Mater.* **2020**, *19* (4), 428–435.
- (34) Sendek, A. D.; Antoniuk, E. R.; Cubuk, E. D.; Ransom, B.; Francisco, B. E.; Buettner-Garrett, J.; Cui, Y.; Reed, E. J. Combining Superionic Conduction and Favorable Decomposition Products in the Crystalline Lithium-Boron-Sulfur System: A New Mechanism for Stabilizing Solid Li-Ion Electrolytes. *ACS Appl. Mater. Interfaces* **2020**, *12* (34), 37957–37966.
- (35) Schwietert, T. K.; Vasileiadis, A.; Wagemaker, M. First-Principles Prediction of the Electrochemical Stability and Reaction Mechanisms of Solid-State Electrolytes. *JACS Au* **2021**, *1* (9), 1488–1496.

- (36) Han, F.; Zhu, Y.; He, X.; Mo, Y.; Wang, C. Electrochemical Stability of Li<sub>10</sub>GeP<sub>2</sub>S<sub>12</sub> and Li<sub>7</sub>La<sub>3</sub>Zr<sub>2</sub>O<sub>12</sub> Solid Electrolytes. *Adv. Energy Mater.* **2016**, *6* (8), 1501590.
- (37) Asakura, R.; Duchêne, L.; Kühnel, R. S.; Remhof, A.; Hagemann, H.; Battaglia, C. Electrochemical Oxidative Stability of Hydroborate-Based Solid-State Electrolytes. *ACS Appl. Energy Mater.* **2019**, *2* (9), 6924–6930.
- (38) Schlueter, C.; Gloskovskii, A.; Ederer, K.; Schostak, I.; Piec, S.; Sarkar, I.; Matveyev, Y.; Lömker, P.; Sing, M.; Claessen, R.; Wiemann, C.; Schneider, C. M.; Medjanik, K.; Schönhense, G.; Amann, P.; Nilsson, A.; Drube, W. The New Dedicated HAXPES Beamline P22 at PETRAIII. *AIP Conf. Proc.* **2019**, *2054*, 040010.
- (39) Ohno, S.; Koerver, R.; Dewald, G.; Rosenbach, C.; Titscher, P.; Steckermeier, D.; Kwade, A.; Janek, J.; Zeier, W. G. Observation of Chemomechanical Failure and the Influence of Cutoff Potentials in All-Solid-State Li-S Batteries. *Chem. Mater.* 2019, 31 (8), 2930–2940.
- (40) Kresse, G.; Furthmüller, J. Efficient Iterative Schemes for Ab Initio Total-Energy Calculations Using a Plane-Wave Basis Set. *Phys. Rev. B Condens. Matter Mater. Phys.* **1996**, *54* (16), 11169–11186.
- (41) Blöchl, P. E. Projector Augmented-Wave Method. *Phys. Rev. B* **1994**, *50* (24), 17953–17979.
- (42) Perdew, J. P.; Ernzerhof, M.; Burke, K. Rationale for Mixing Exact Exchange with Density Functional Approximations. *J. Chem. Phys.* **1996**, *105* (22), 9982–9985.
- (43) Heyd, J.; Scuseria, G. E. Efficient Hybrid Density Functional Calculations in Solids: Assessment of the Heyd–Scuseria–Ernzerhof Screened Coulomb Hybrid Functional. *J. Chem. Phys.* **2004**, *121* (3), 1187–1192.
- (44) Jain, A.; Ong, S. P.; Hautier, G.; Chen, W.; Richards, W. D.; Dacek, S.; Cholia, S.; Gunter, D.; Skinner, D.; Ceder, G.; Persson, K. A. Commentary: The Materials Project: A Materials Genome Approach to Accelerating Materials Innovation. APL Mater. 2013, 1 (1), 011002.
- (45) Jain, A.; Hautier, G.; Moore, C. J.; Ping Ong, S.; Fischer, C. C.; Mueller, T.; Persson, K. A.; Ceder, G. A High-Throughput Infrastructure for Density Functional Theory Calculations. *Comput. Mater. Sci.* 2011, 50 (8), 2295–2310.

- (46) Ong, S. P.; Richards, W. D.; Jain, A.; Hautier, G.; Kocher, M.; Cholia, S.; Gunter, D.; Chevrier, V. L.; Persson, K. A.; Ceder, G. Python Materials Genomics (Pymatgen): A Robust, Open-Source Python Library for Materials Analysis. *Comput. Mater. Sci.* 2013, 68, 314–319.
- (47) Cao, D.; Zhang, Y.; Nolan, A. M.; Sun, X.; Liu, C.; Sheng, J.; Mo, Y.; Wang, Y.; Zhu,
  H. Stable Thiophosphate-Based All-Solid-State Lithium Batteries through
  Conformally Interfacial Nanocoating. *Nano Lett.* 2020, 20 (3), 1483–1490.
- (48) Zhu, Y.; He, X.; Mo, Y. Strategies Based on Nitride Materials Chemistry to Stabilize Li Metal Anode. *Adv. Sci.* **2017**, *4* (8), 1600517.
- (49) Ong, S. P.; Wang, L.; Kang, B.; Ceder, G. Li-Fe-P-O<sub>2</sub> Phase Diagram from First Principles Calculations. *Chem. Mater.* **2008**, *20* (5), 1798–1807.
- (50) Maintz, S.; Deringer, V. L.; Tchougréeff, A. L.; Dronskowski, R. LOBSTER: A Tool to Extract Chemical Bonding from Plane-Wave Based DFT. J. Comput. Chem. 2016, 37 (11), 1030–1035.
- (51) Deringer, V. L.; Tchougréeff, A. L.; Dronskowski, R. Crystal Orbital Hamilton Population (COHP) Analysis As Projected from Plane-Wave Basis Sets. *J. Phys. Chem. A* 2011, 115 (21), 5461–5466.
- (52) Dewald, G. F.; Ohno, S.; Hering, J. G. C.; Janek, J.; Zeier, W. G. Analysis of Charge Carrier Transport Toward Optimized Cathode Composites for All-Solid-State Li–S Batteries. *Batter. Supercaps* **2021**, *4* (1), 183–194.
- (53) Deiseroth, H.-J.; Maier, J.; Weichert, K.; Nickel, V.; Kong, S.-T.; Reiner, C. Li<sub>7</sub>PS<sub>6</sub> and Li<sub>6</sub>PS<sub>5</sub>X (X: Cl, Br, I): Possible Three-Dimensional Diffusion Pathways for Lithium Ions and Temperature Dependence of the Ionic Conductivity by Impedance Measurements. *Zeitschrift für Anorg. und Allg. Chemie* **2011**, *637* (10), 1287–1294.
- (54) Boulineau, S.; Courty, M.; Tarascon, J.-M.; Viallet, V. Mechanochemical Synthesis of Li-Argyrodite Li<sub>6</sub>PS<sub>5</sub>X (X=Cl, Br, I) as Sulfur-Based Solid Electrolytes for All Solid State Batteries Application. *Solid State Ionics* **2012**, *221*, 1–5.
- (55) Zhou, L.; Park, K.-H.; Sun, X.; Lalère, F.; Adermann, T.; Hartmann, P.; Nazar, L. F. Solvent-Engineered Design of Argyrodite Li<sub>6</sub>PS<sub>5</sub>X (X = Cl, Br, I) Solid Electrolytes with High Ionic Conductivity. *ACS Energy Lett.* **2019**, *4* (1), 265–270.

(56) Haque, A.; Banik, A.; Varma, R. M.; Sarkar, I.; Biswas, K.; Santra, P. K. Understanding the Chemical Nature of the Buried Nanostructures in Low Thermal Conductive Sb-Doped SnTe by Variable-Energy Photoelectron Spectroscopy. *J. Phys. Chem. C* 2019, *123* (16), 10272–10279.

# **TOC Graphic**

